Quantum walk and random walk behaviors of

dressed-photon-phonon transfers

M. Ohtsu

Research Origin for Dressed Photon, 3-13-19 Moriya-cho, Kanagawa-ku, Yokohama, Kanagawa 221-0022, Japan

Abstract

This paper reviews measured results on the temporal variation behavior of the dressed photon (DP) transfers between nanometer-size particles (NPs). The NPs are illuminated with a short optical pulse, and the resulting behavior of the emitted photoluminescence (PL) intensity is evaluated. Even after the optical pulse is turned off, the PL intensity exhibits nutation within a short time span. The envelope intensity of the nutation decreases due to adiabatic and non-adiabatic processes. They are described by using a quantum walk (QW) model and a random walk (RW) model, respectively. It is revealed that the values of several relevant quantities in these models must be adjusted in an appropriate manner to clearly observe the DP transfer features. The rate of conversion from the adiabatically dissipated energy to the non-adiabatically dissipated energy must also be adjusted. An antenna system composed of photosynthetic bacteria is presented, suggesting that a future direction of DP research is to draw a universal physical picture of DP transfers that are commonly found in nature.

1 Introduction

A dressed photon (DP) is a quantum field that is created by a photon–exciton (or electron) interaction in a nanometer-sized particle (NP). Recent theoretical studies on off-shell science have succeeded in drawing a precise physical picture of the DP creation process [1,2]. Furthermore, intensive experimental studies have confirmed that a dressed-photon–phonon (DPP) is created by DP–phonon coupling. These studies have also revealed a unique DPP transfer behavior between adjacent NPs, which was used to develop a variety of innovative technologies [3,4].

This paper indicates that short and long time-span temporal variations of the DPP transfer exhibit unique behaviors that can be described by quantum walk (QW) and random walk (RW) models.

2 Revisiting experimental results

This section reviews the experimentally confirmed temporal variation behaviors of the DPP transfer. Here, the DPP is replaced by a DP because the phonons in the DPP do not give any noticeable contributions to characterize the temporal variation behavior. Several features of these behaviors have been analyzed by using QW models [5–7]¹⁾.

- 1) The reason why this analysis is possible is that the principles of the QW model and the nature of the DP have at least two features in common [7]:
- (A) Nonreciprocity: A mathematical formulation of the QW uses nonreciprocal algebra involving vectors and matrices. On the other hand, the DP is a field that mediates the interaction between NPs. Since the interaction is a typical nonreciprocal physical process, the QW and DP have a common feature, represented by nonreciprocity.
- (B) Site: The QW deals with the phenomenon of the energy transfer from one site to its neighbor. On the other hand, since the DP is spatially localized, its quantum mechanical position operator can be defined. Thus, in the case where the site of the QW is the NP on which the DP is created, the position of the DP is equivalent to that of the site of the QW.

2.1 Basic properties of temporal variation [8]

Figure 1(a) shows a pair of cubic CuCl NPs grown in a NaCl crystal. A small NP (NPs) and a large NP (NP_L) correspond to nodes 1 and 2 in the QW model in Fig. 1(b). The DP transfers between these NPs and plays the role of a link in this model. The incident light (an optical pulse; pulse width of 10 ps and wavelength of 381 nm) in Fig. 1(a) corresponds to the input signal in Fig. 1(b). The created excitons in NP_S and NP_L emit photoluminescences (PL₁ and PL₂) that correspond to the output signals 1 (wavelength of 382 nm) and 2 (wavelength of 385 nm).

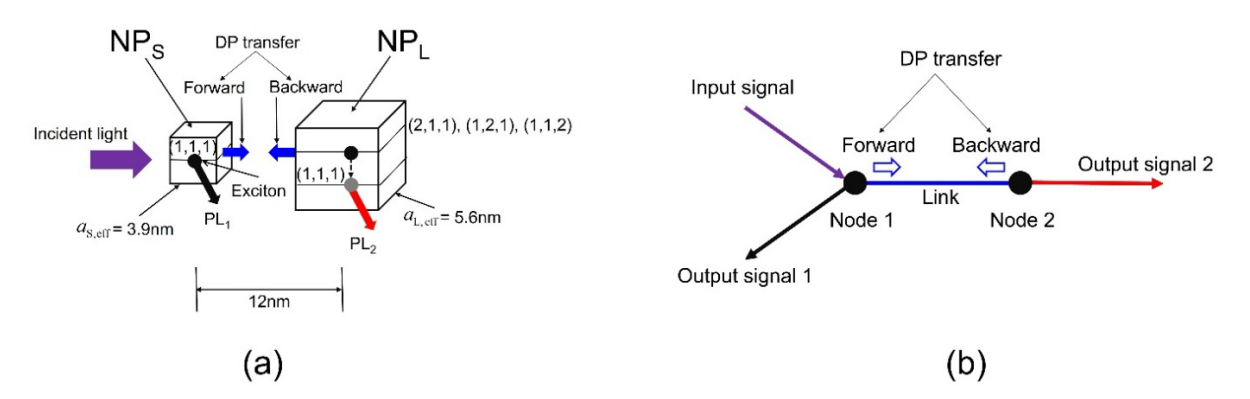


Fig. 1 A pair of NPs composed of small and large NPs (NPs and NPL).

(a) Experimental system. The exciton in NP_L has triply degenerate energy levels. (b) QW model.

The output signals are created by five successive steps. They are:

- (Step 1) The incident light creates an exciton in the energy level (1,1,1) of NP_S.
- (Step 2) This exciton emits PL_1 (the output signal 1) and also creates a DP.
- (Step 3) The created DP transfers to the NP_L to excite an exciton in the triply degenerate energy levels (2,1,1), (1,2,1), and (1,1,2) of NP_L.
- (Step 4) This exciton creates a DP, and the created DP transfers back to the NPs.
- (Step 5) This exciton is also de-excited to the lower energy level (1,1,1) of NP_L and subsequently emits PL₂ (the output signal 2).

As long as the incident light is applied, these five steps repeat, and the DP repeatedly transfers between NP_S and NP_L in a bi-directional manner (**Step 4**); this is called nutation. In the case where the incident light is an optical pulse, this bi-directional transfer is maintained within a short time-span even after the incident optical pulse is turned off. Thus, the intensities of PL_1 and PL_2 continue to pulsate due to the DP nutation.

However, these intensities gradually decrease due to non-radiative energy dissipation to the heat bath (the NaCl crystal), so that PL₁ and PL₂ fade away. This dissipation is composed of adiabatic and non-adiabatic processes. The former is the process in which the exciton in NP_s or NP_L excites other excitons (or electrons) in another NP or in the heat bath. The latter is the process in which the exciton energy is converted to thermal energy and is dissipated in the heat bath. The magnitude of the latter process depends on the device temperature, and the time constant of the PL intensity variation is longer than that due to the former process. Although these adiabatic and non-adiabatic processes contribute to the intensities of the outputs 1 and 2, the ratio of the magnitudes of these contributions has not been precisely evaluated by measurements. Theoretical studies are required to evaluate it.

The wavelength (385 nm) of the output signal 2 (PL₂) is longer than that of the output signal 1 (PL₁, 383 nm) because a part of the energy is dissipated from the triply degenerate energy level during the de-excitation to the lower energy level (1,1,1). Even though the magnitude of this dissipated energy is as low as 1/100 times the photon energy of the output signal 1, it is sufficiently large to spectrally resolve the output signals 1 and 2 for separate measurements.

Figure 1(b) can be redrawn as Fig. 2(a) by noting the triple degeneracy of the exciton energy levels in NP_L and the energy dissipation from these levels during the de-excitation to (1,1,1). For basic discussions of the QW process, Fig. 2(a) can be approximated by the simpler system in Fig. 2(b) because of the sufficiently low magnitude of the energy dissipation above.

Since the sizes, $a_{\rm S}$ and $a_{\rm L}$, of NP_S and NP_L are different from each other, the magnitudes of the created DP energies and their spatial extents are different, as represented by a Yukawa-type function V(r) ($\propto \exp(-r/a)/r$, where a is the size of the NP). Thus, because the time required for the DP transfer is inversely proportional to V(r), the transfer times along the forward path (NP_S to NP_L) and backward path (from NP_L to NP_S) are different from each other.

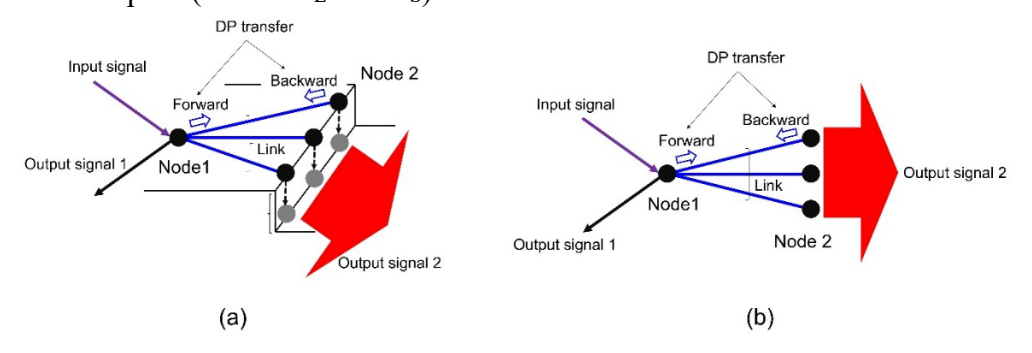


Fig. 2 The revised QW system.

For basic discussion, (a) is approximated by (b).

The black and red curves in Fig. 3(a) represent the measured temporal variations of PL₁ and PL₂ (the output signals 1 and 2), respectively. In the short time-span 0–500 ps immediately after applying the pulsed input signal, the intensity decrease is attributed to the adiabatic process and is fitted by $\exp(-t/\tau_{f1})$ (blue line) of the QW model, where τ_{f1} is the decay time constant. The subsequent decrease in the long time-span from 500 ps to 4 ns is slower and is fitted by $\exp(-\sqrt{t/\tau_{f2}})$ (red line) of the RW model, which is attributed to the non-adiabatic process [9]. The decay time constant τ_{f2} is longer than τ_{f1} .

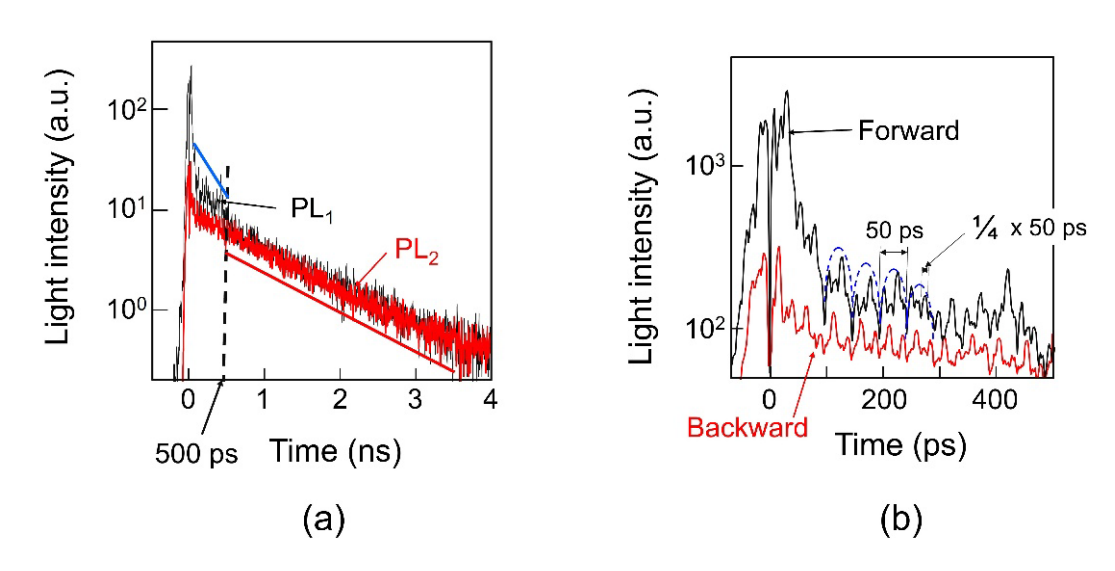


Fig. 3 The measured temporal variations of the PL₁ and PL₂ intensities.

(a) For the short time-span of 0-4 ns. The blue and red lines represent $\exp(-t/\tau_{f1})$ and $\exp(-\sqrt{t/\tau_{f2}})$, respectively.

(b) For the long time-span of 0-500 ps. The black and red curves indicate the temporal variations of the DP transfer along the forward and backward paths, respectively.

2.2 Characteristics caused by triple degeneracy [8]

Since the present paper focuses on the phenomena relevant to the QW process, Fig. 3(b) is presented by expanding the horizontal axis of Fig. 3(a) to analyze the temporal variations in the time-span 0–500 ps. The black and red curves indicate the magnified temporal variations of the DP energy transfer along the forward and backward paths, respectively. Their pulsatory variations represent nutation with a period of 50 ps. This value is compatible with the cycle time of 40 ps that was estimated from the relation between the NP_S–NP_L distance (10 nm) and the transferred DP energy $(1 \times 10^{-4} \text{ eV})$ [10].

Figure 3(b) indicates inherent characteristics of DP transfer caused by the triple degeneracy of the exciton energy levels in NP_L. They are:

(Characteristic 1) The phases of the pulsatory variations of the two curves are different from each other. In order to derive the magnitude of this difference, the nutation components of the 50 ps-period are extracted from these curves and are shown in Fig. 4. The sinusoidal black curve has a phase lag of $\pi/3$ behind that of the red curve. This is because the triple degeneracy caused a lag of one-third of π^{2} . That is, within one-third of the DP transfer time along the backward path, the energy level (1,1,1) in NP_S is promptly occupied by the exciton that is initially created in the triply degenerate energy levels in NP_L³).

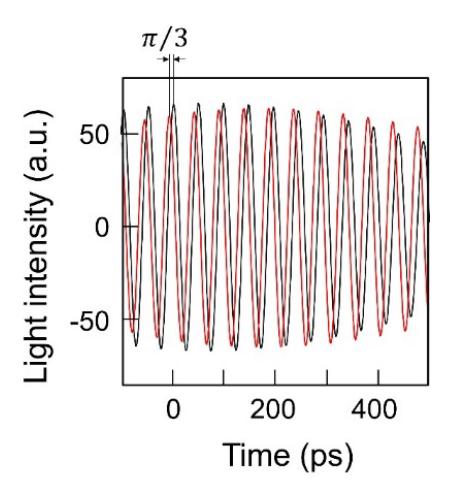


Fig. 4 Fourier components of the measured temporal variations of PL₁ and PL₂. The nutation components with a 50 ps period were extracted from the black and red curves in Fig. 3(b).

(Characteristic 2) Blue broken curves in Fig. 3(b) represent that the pulsatory variations of the PL intensities are modulated. This is attributed to the fact that the transfer times along the forward path and along the backward path are different from each other.

(Characteristic 3) Additional pulsatory variations exist, the period of which is one-fourth that of the nutation. Such a short period is attributed to the fact that, among the four energy levels (level (1,1,1) in NP_S and the triply degenerate energy levels in NP_L), only the energy level (1,1,1) in NP_S is initially occupied by an exciton at the commencement of the nutation.

Figure 5 shows the Fourier spectral profiles of the two curves in Fig. 3(b). The spectral peak (A) at 20 GHz corresponds to the nutation period of 50 ps. Because the profiles of the measured pulsatory variations deviate from sinusoidal curves, the spectral peak (B) of the second-order higher harmonic can be seen. The spectral peak of the third-order higher harmonic is missing due to the difference between the forward and backward transfer times. The spectral peak (C) is attributed to the superposition of the fourth-order higher harmonic and the additional pulsatory variations whose period is one-fourth of the nutation cycle.

Sections 2.3 and 2.4 will review temporal variations observed in other experimental systems that were used to develop practical devices. The effect of the triple degeneracy can be neglected in these sections because of its minor contribution to these systems.

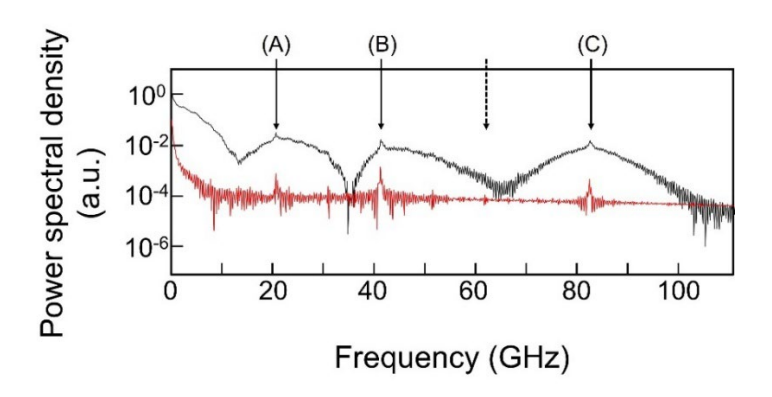


Fig. 5 The Fourier spectral profiles of the two curves in Fig. 3(b).

Spectral peaks A and B correspond to the nutation of the 50 ps period and its second-order higher harmonic. The peak C is attributed to the superposition of the fourth-order higher harmonic and the additional pulsatory variations.

- 2) This kind of phase lag has never been observed when using a large number of NPs as the macroscopic material system for inducing conventional optical phenomena. This is because the NPs in this system have been approximated as a coupled quantum state having a singlet state of the exciton.
- 3) Since the DP transferred bi-directionally between NP_S and NP_L, the profiles of the two curves in Fig. 4 should be anti-correlated, and thus, their phase difference should be as large as π . However, the phase lag was found to be $\pi/3$. The reason for this discrepancy was considered to be as follows: Since a large number of CuCl NPs were buried in the NaCl crystal, the DP could transfer not only between NP_S and NP_L but also between multiple NP_Ls (or between multiple NP_Ss). Furthermore, since the number of NP_Ls was larger than the number of NP_Ss, the DP transfer between neighboring NP_Ls could contribute to the phase difference between the two curves. However, since the phase of the DP transfer between these NP_Ls is random, the anti-correlation characteristics did not clearly appear, and thus, the phase difference remained as small as $\pi/3$.

2.3 DP transfer in nanometer-sized devices [11]

Nano-optical condenser [12]: Figure 6(a) schematically explains the structure of a nano-optical condenser device. Three kinds of cubic CuCl NPs (NPs, NP_M, and NP_L) grown in a NaCl crystal are used: A large NP (NP_L) is surrounded by a large number of small NPs (NP_S). Medium-sized NPs (NP_M) are placed in the spaces between the NP_Ss and the NP_L.

This device uses DP transfers from the NP_Ss to the NP_M and subsequently to the NP_L for collecting the incident optical energy at the NP_L. As a result, the output signal of a sub-wavelength-sized (20 nm-diameter) spot is emitted from the NP_L, as is demonstrated by Fig. 6(b). Figure 6(c) shows the measured spatial and temporal variations of the light intensity, from which one can find that the energy is collected at NP_L within a time as short as 1 ns. Since this variation behavior reminds one of a fountain of gushing water (Fig. 6(d)), this device is called an optical nano-fountain.

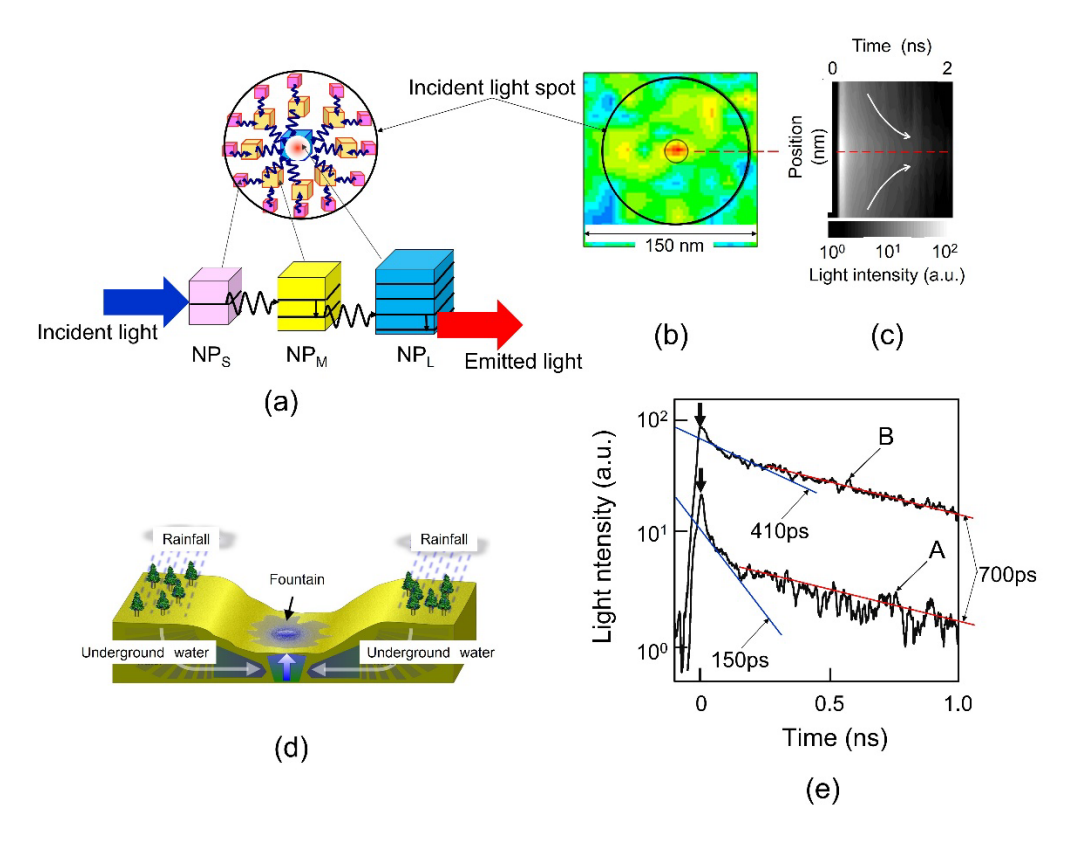


Fig. 6 Nano-optical condenser (Optical nano-fountain).

(a) The device structure. (b) and (c) are the measured spatial distribution and temporal variation of the emitted light intensity, respectively. (d) Schematic explanation of the fountain. (e) Measured temporal variation of the emitted light intensities. Curves A and B represent the intensities, emitted from NP_Ms and NP_L, respectively. The peaks at t = 0, identified by the downward arrows, represent artifacts originating from the incident optical pulse. Blue and red lines represent $\exp(-t/\tau_{f1})$ and $\exp(-\sqrt{t/\tau_{f2}})$, respectively.

Figure 6(e) shows the measured relation between time (t) and the light intensity emitted from the device when it was illuminated by a short optical pulse of 325 nm-wavelength at t=0. Curve A is the intensity of the light emitted from the NP_Ms as a result of the DP transfer from the NP_Ss to the NP_Ms and subsequent energy dissipation of the excitons in the NP_Ms. Curve B is the intensity of the light that is finally emitted from the NP_L. It is confirmed that the light is efficiently collected at NP_L by noting that the value of curve B is more than ten times that of curve A. The peaks of these curves at t=0, identified by the downward arrows, represent artifacts originating from the incident optical pulse.

The profiles of curves A and B are similar to those of the curves in Fig. 3(a). They have two time constants that originate from the adiabatic and non-adiabatic processes. The former is the constant τ_{f1} in $\exp(-t/\tau_{f1})$ (blue line) whose values are 150 ps and 410 ps for curves A and B,

respectively. The latter is the constant τ_{f2} in $\exp(-\sqrt{t/\tau_{f2}})$ (red line) whose value is 700 ps for both curve A and curve B.

Optical buffer memory [13]: Figure 7(a) schematically explains the structure of an optical buffer memory device. For holding the input signal in this device, DP nutation between two NPs of the same size (two blue cubes) is used. The buffering time corresponds to the cycle time of the nutation. To read out the held signal, a NOT logic gate, whose operation is based on the DP transfer, is installed in proximity to the two NPs. Application of a readout optical pulse to the NOT logic gate creates an output signal.

Figure 7(b) is the temporal variation of the output signal intensity plotted as a function of the time delay defined as the time difference between the application of the input and readout pulses to the device. Curves A and B represent the measured values. Curve C is the theoretical curve fitted to them by using three values: τ_{f1} of 600 ps, τ_{f2} of 1300 ps, and a nutation cycle of 155 ps. Curve C exhibits a pulsating behavior that takes a first local maximum immediately after the readout pulse is applied. This corresponds to the first output signal. Subsequently, a series of output signals repeatedly appears with a period of 150 ps, which corresponds to the nutation cycle above.

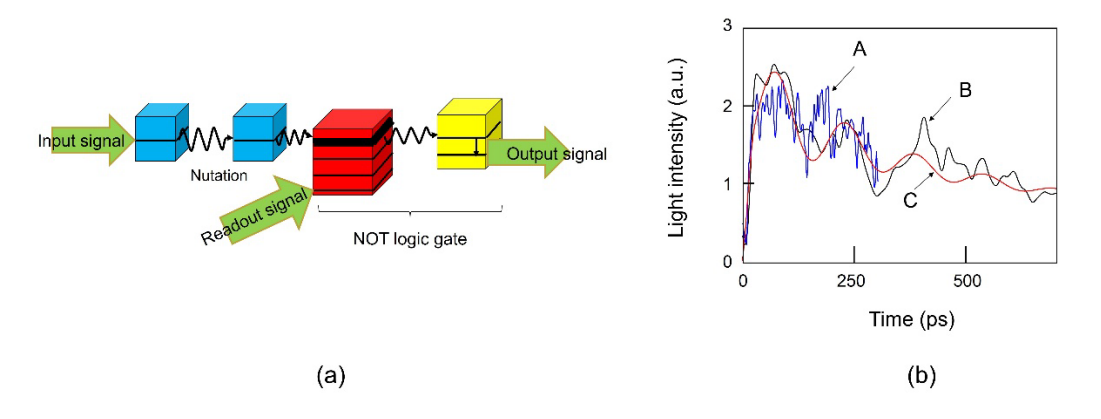


Fig. 7 Optical buffer memory device.

(a) The device structure. (b) Temporal variation of the output signal intensity as a function of the time delay. Curves A and B represent the measured results. Curve C is the theoretical curve fitted to the curves A and B.

2.4 DP transfer between different kinds of NPs [14,15]

Even when the two CuCl NPs (NPs and NP_L in Fig. 1(a)) are replaced by different kinds of NPs, the DP exhibits temporal variation similar to Fig. 3. This suggests that the DP transfer is a universal phenomenon that can be observed in a variety of NP-systems in the natural world. For example, experiments have been carried out by using a pair of NPs composed of a semiconductor ZnO NP and a dye-molecular DCM NP. In this case, electrons in these NPs play the role of the excitons in CuCl NPs.

The left and right parts of Fig. 8 show the electron energy levels of ZnO NP and DCM NP, respectively. Photoluminescence is emitted from electrons in these levels. The measured results are indicated by curves A, B, and C in Fig. 9(a).

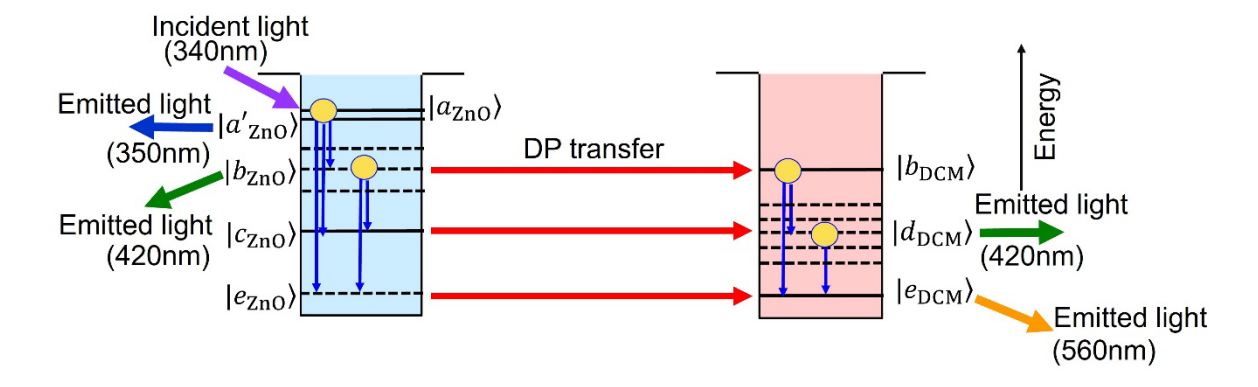


Fig. 8 Electron energy levels of ZnO NP (left) and DCM NP (right). The wavelength of the emitted light is shown in the parenthesis.

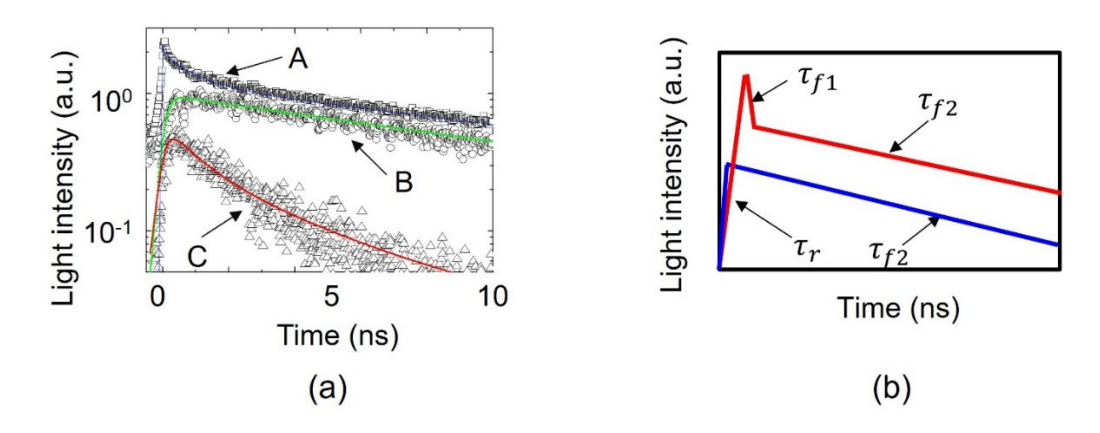


Fig. 9 Temporal evolutions of the emitted light intensities.

(a) Measured values. (b) Schematic explanation of the curves in (a).

The identities of these curves are:

Curve A: The light intensity (wavelength 350 nm) that is emitted from the electron in the energy level $|a'_{ZnO}\rangle$ of the ZnO NP. The wavelength of the incident light is 340 nm, which is resonant with the energy level $|a_{ZnO}\rangle$.

Curve B: The light intensity (wavelength 560 nm) that is emitted from the electron in the energy level $|e_{DCM}\rangle$ of the DCM NP. The wavelength of the incident light is 340 nm, which is resonant with the energy level $|a_{Z_{RQ}}\rangle$.

Curve C: The light intensity (wavelength 420 nm) that is emitted from the electron in the energy levels $|b_{ZnO}\rangle$ and $|d_{DCM}\rangle$ of the ZnO NP and the DCM NP, respectively. The wavelength of the incident light is 420 nm, which is resonant with the energy level $|c_{ZnO}\rangle$ in the ZnO NP.

Figure 9(b) is a schematic explanation of the curves in Fig. 9(a). The red zigzag line corresponds to curve A in Fig. 9(a). The rise-up time constant is represented by τ_r , that is 100-150 ps in Fig. 9(a). The rapid decrease of curve A in a short time-span is attributed to the adiabatic process. It is represented by a short time constant τ_{f1} of the red zigzag line. Its value is nearly equal to τ_r of Fig. 9(a). The subsequent slow decrease is attributed to the non-adiabatic process, whose time constant τ_{f2} is as long as 15 ns in Fig. 9(a). The blue zigzag line corresponds to curves B and C in Fig. 9(a). Its rise-up time constant τ_r is equal to that of the red zigzag line. Since curves B and C do not show rapid decreases with the time constant τ_{f1} , they are represented only by the slowly decreasing blue zigzag line in Fig. 9(b) with the long time constant τ_{f2} .

3 Theoretical models for describing temporal variation behaviors of the output signals.

The features of the experimental results and theoretical models in Section 2 can be summarized as follows:

- (1) The output signal intensity pulsates in a short time-span immediately after the pulsive input signal is applied. This pulsation is called nutation. The signal intensity rapidly decreases with a short time constant that is attributed to the adiabatic process and is fitted by $y_{QR} = a_{QW} \exp(-t/\tau_{QW})$ based on the QW model. Here, since this process is compatible with the QW model, the time constant τ_{f1} in Section 2 is rewritten as τ_{QW} .
- (2) In a long time-span, the output signal intensity decreases slowly due to a non-adiabatic process that is fitted by $y_{RW} = a_{RW} \exp(-\sqrt{t/\tau_{RW}})$ based on the RW model. Here, since this process is compatible with the RW model, the time constant τ_{f2} in Section 2 is rewritten as τ_{RW} .

Measured values of nutation cycle and time constants are summarized in Table 1. This table indicates that the time constant τ_{QW} is shorter than τ_{RW} . That is, $\tau_{QW}/\tau_{RW} = 6.7 \times 10^{-3}$ - 0.58 and is expressed as

$$\tau_{OW}/\tau_{RW} < 1. \tag{1}$$

Table 1 Measured values of nutation cycle and time constants.

- *) The nutation cycle of 400 ps was also measured for an optical switching device that was composed of CuCl NPs [15].
- **) The time constants $\ au_{f1}$ and $\ au_{f2}$ in Section 2 are rewritten as $\ au_{QW}$ and $\ au_{RW}$, respectively.

	Nutation cycle*)	$ au_r$	$ au_{\mathit{QW}}^{\ \ **)}$	$ au_{\scriptscriptstyle RW}^{ **)}$
Section 2.2	50 ps			
Section 2.3				
Nano-optical condenser	155 ps		150 ps, 410 ps	700 ps
Optical buffer memory			600 ps	1,300 ps
Section 2.4		100-150 ps	100-150 ps	15 ns

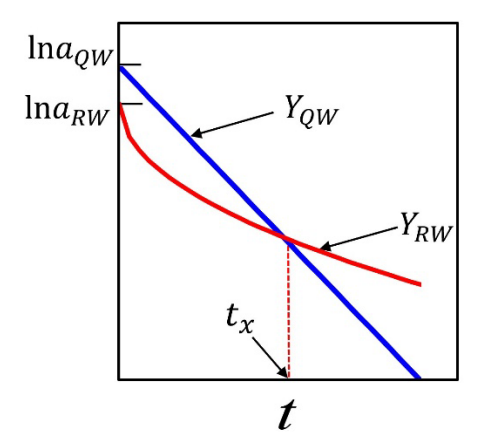


Fig. 10 Temporal variations of eqs. (2) (blue line) and (3) (red curve).

Temporal variations of the exponential functions in (1) and (2) are schematically explained by Fig. 10, in which the vertical axis is indicated on a logarithmic scale:

$$Y_{QW} = \ln y_{QW} = \ln a_{QW} - t / \tau_{QW},$$
 (2)

and

$$Y_{RW} = \ln y_{RW} = \ln a_{RW} - \sqrt{t/\tau_{RW}}$$
 (3)

Due to the small value of τ_{QW}/τ_{RW} , the slope of the blue line (Y_{QW}) in this figure is steeper than that of the red curve (Y_{RW}) . The value of a_{RW} is assumed to be smaller than that of a_{QW} $(a_{RW}/a_{QW}<1)$ by referring to the curves in Figs. 3(a), 6(e), 7(b), and also curve A in Fig. 9(a).

This figure indicates that the QW feature can be clearly observed in the early short time-span because the signal intensity of Y_{QW} (blue line) is larger than that of Y_{RW} (red curve). However, after that, this feature is obscured by the RW feature (red curve) due to the rapid decreases of Y_{QW} . The time at which the blue line and red curve cross is represented by t_x in this figure.

For making full use of the output signal originating from the DP transfer for device applications⁴⁾, a sufficiently long crossing time t_x is required to ensure a time during which the QW features can be clearly observed. To meet this requirement, the values of a_{RW}/a_{QW} and τ_{QW}/τ_{RW} must be adjusted in an appropriate manner. It should be noted that the values of a_{RW} and τ_{RW} depend on the device temperature T (they are proportional to T and T^{-1} , respectively).

⁴⁾ Since curves B and C in Fig. 9(a) correspond the case of $a_{RW}/a_{QW} > 1$, the QW features are obscured by the RW features and are not advantageous for practical applications.

Furthermore, it should be pointed out that a part of the adiabatically dissipated energy may be converted to non-adiabatically dissipated energy. Even though this conversion mechanism has not yet been precisely evaluated by experiments, the exponential functions y_{QR} and y_{RW} should be revised to

$$\dot{y}_{QW} = (1 - \varepsilon) a_{QW} \exp(-t / \tau_{QW}) \tag{4}$$

and

$$y_{RW} = \left(a_{RW} + \varepsilon a_{OW}\right) \exp\left(-\sqrt{t/\tau_{RW}}\right),\tag{5}$$

respectively, by referring to this conversion. Here, ε (<<1) is the conversion rate. In order to maintain

the long time t_x , the value of ε must also be adjusted in an appropriate manner. It can be assumed that this value can be optimized for maximizing the output signal intensity by means of the adjustment above. Such an optimum value has been discussed in the case of the QW model [16]. The example is the optimum value κ_{opt} of the dispersion constant κ for maximizing the output signal, as is shown by Fig. 11.

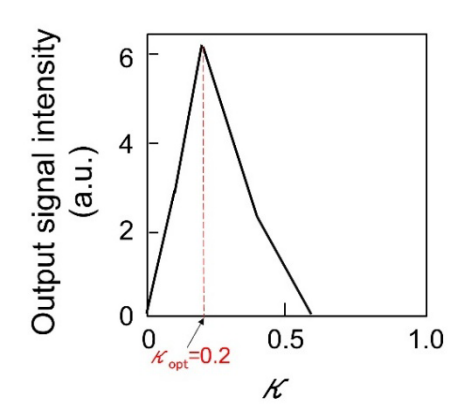


Fig. 11 Relation between the dissipation constant κ and the output signal intensity [16].

4 Future directions

DP transfer is presumed to be a universal phenomenon that can be observed in a variety of NPs in the natural world. To demonstrate an example of such universality, Fig. 12 schematically explains the structure of an antenna system that is composed of photosynthetic bacteria [17], by which solar energy is collected at the reaction center. Here, the essential problem is that the excitation energy transfer (ETT) process in this system has not yet been precisely analyzed using traditional Förster theory. This is because this theory is based on the primitive concept of electric-dipole transitions and the long-wavelength approximation. Detailed studies are in progress to solve this problem by improving the accuracy of the theory [18].

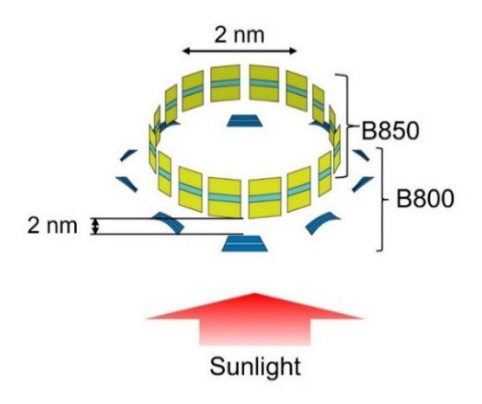


Fig. 12 The structure of an antenna system made of photosynthetic bacteria [17].

This problem may be solved if the theoretical model of DP creation [1,2] and the QW model for DP transfer [5-7] are used because the DP creation and transfer processes have several equivalences with the ETT process. Actually, the motivation for inventing the nano-optical condenser (optical nano-fountain) in Fig. 6 was to build a practical semiconductor device to realize a function equivalent to that of the system in Fig. 12 [12]. Experiments have already confirmed that this device succeeded in collecting the incident optical energy at NP_L at the center.

By referring to the example above, one of the promising directions of future DP research is to discover a route to the precise analysis of the DP transfer phenomena, not only in physical and chemical systems but also in biological systems and other systems. For reference, novel features such as hierarchy [19] and autonomy [20, 21] have been found in the DP transfer, and these features have several equivalences with biological signal transmission processes in neurons.

5 Summary

This paper reviewed the measured results of the temporal variation behavior of the DP transfer between NPs. By illuminating the NPs with a short optical pulse, the temporal variation of the emitted PL intensity was evaluated. Even after the optical pulse was turned off, the PL intensity exhibited nutation within a short time-span. The envelope intensity of the nutation decreased due to adiabatic and non-adiabatic processes. They were described by using a QW model and a RW model, respectively. It was pointed out that the values of several relevant quantities in these models must be adjusted in an appropriate manner to clearly observe the DP transfer features. The rate of conversion from the adiabatically dissipated energy to the non-adiabatically dissipated one must also be adjusted.

An antenna system composed of photosynthetic bacteria was presented for demonstrating the ETT process that is equivalent to those of the DP creation and transfer. It was suggested that future research of DPs will involve analyzing this process and building more precise theoretical models for drawing a universal physical picture of the DP transfers that are commonly found in nature.

References

- [1] M. Ohtsu and H. Sakuma, Dressed Photons to Revolutionize Modern Physics (Springer, Heidelberg, 2025) 65-118.
- [2] H. Sakuma, I. Ojima, and M. Ohtsu, "Perspective on an Emerging Frontier of Nanoscience Opened up by Dressed Photon Studies," *Nanoarchitectonics*, Vol. 5, Issue 1 (2024) 1-23.
- [3] M. Ohtsu, Dressed Photons (Springer, Heidelberg, 2014) 89-214.
- [4] M. Ohtsu, Silicon Light-Emitting Diodes and Lasers (Springer, Heidelberg, 2016) 1-138.
- [5] M. Ohtsu, Off-Shell Applications in Nanophotonics (Elsevier, Amsterdam, 2021) 162-165.
- [6] M. Ohtsu and H. Sakuma, Dressed Photons to Revolutionize Modern Physics (Springer, Heidelberg, 2025)41-64.
- [7] M. Ohtsu, "Off-shell scientific nature of dressed photon energy transfer and dissipation," Off-shell Archive (April, 2024) Offshell: 2404R.001.v1. **DOI** 10.14939/2404R.001.v1, https://rodrep.or.jp/en/off-shell/review 2404R.001.v1.html
- [8] M. Ohtsu and T. Kawazoe, "Nutation in energy transfer of dressed photons between nano-particles," Off-shell Archive (May, 2020) Offshell: 2005O.001.v1. **DOI** 10.14939/2005O.001.v1,

- https://rodrep.or.jp/en/off-shell/original 2005O.001.v1.html
- [9] H. Saigo, Quantum Probability for Dressed Photons: The Arcsine Law in Nanophotonics, *Prog. in Nanophotonics 5* (ed. T. Yatsui) (Springer, Heidelberg, 2018) 79-106.
- [10] T. Kawazoe, K. Kobayashi, J. Lim, Y. Narita, and M. Ohtsu, "Direct Observation of Optically Forbidden Energy Transfer between CuCl Quantum Cubes via Near-Field Optical Spectroscopy," *Phys. Rev. Lett.*, **88** (2002) 067404.
- [11] M. Ohtsu, "Novel functions and prominent performance of nanometric optical devices made possible by dressed photons," Off-shell Archive (April, 2019) Offshell: 1904R.001.v1. **DOI** 10.14939/1904R.001.v1, https://rodrep.or.jp/en/off-shell/review 1904R.001.v1.html
- [12] T. Kawazoe, K. Kobayashi, and M. Ohtsu, "Optical nanofountain: A biomimetic device that concentrates optical energy in a nanometric region", *Appl. Phys. Lett.*, **86** (2005) 103102.
- [13] M. Ohtsu, Off-Shell Applications in Nanophotonics (Elsevier, Amsterdam, 2021) 58-59.
- [14] M. Ohtsu, Off-Shell Applications in Nanophotonics (Elsevier, Amsterdam, 2021) 95-101.
- [15] M. Ohtsu, T. Kawazoe, and H. Saigo, "Spatial and temporal evolutions of dressed photon energy transfer," Offshell Archive (October, 2017) Offshell: 1710R.001.v1. **DOI** 10.14939/1710R.001.v1, https://rodrep.or.jp/en/off-shell/review 1710R.001.v1.html
- [16] M. Ohtsu, E. Segawa, K. Yuki, and S. Saito, "Optimum dissipation for governing the autonomous transfer of dressed photons," *Off-shell Archive* (May, 2025) Offshell: 2405O.001.v1.
- **DOI** 10.14939/2405O.001.v1, https://rodrep.or.jp/en/off-shell/original 2405O.001.v1.html
- [17] H.-M. Wu, N.R.S. Reddy, and G.J. Small, "Direct observation and hole burning of the lowest exciton level (B870) of the LH2 antenna complex of *Rhodopseudomonas acidophila*," *J. Phys. Chem.*, B101 (1996) pp.651-656.
- [18] H. Sumi, "Theory on rates of excitation-energy transfer between molecular aggregates through distributed transition dipoles with application to antenna system in bacterial photosynthesis," *J. Phys. Chem.*, B**103** (1996) pp.252-260.
- [19] M. Ohtsu and H. Sakuma, Dressed Photons to Revolutionize Modern Physics (Springer, Heidelberg, 2025) 29-31.
- [20] M. Ohtsu, Off-Shell Applications in Nanophotonics (Elsevier, Amsterdam, 2021) 54-55.
- [21] M. Ohtsu and H. Sakuma, Dressed Photons to Revolutionize Modern Physics (Springer, Heidelberg, 2025) 31-33.